Inorganics **2014**, *2*, 396-409; doi:10.3390/inorganics2030396

OPEN ACCESS

inorganics

ISSN 2304-6740

www.mdpi.com/journal/inorganics

Review

Nanostructured Boron Nitride: From Molecular Design to Hydrogen Storage Application

Georges Moussa [1], Chrystelle Salameh [1], Alina Bruma [2], Sylvie Malo [2], Umit B. Demirci [1], Samuel Bernard [1,*] and Philippe Miele [1]

[1] IEM (Institut Europeen des Membranes), UMR 5635 (CNRS-ENSCM-UM2), Universite Montpellier 2, Place E. Bataillon, F-34095 Montpellier, France; E-Mails: georges_moussa@hotmail.com (G.M.); chrystelle.salameh@univ-montp2.fr (C.S.); umit.demirci@univ-montp2.fr (U.B.D.); philippe.miele@univ-montp2.fr (P.M.)

[2] Laboratoire CRISMAT, UMR 6508 CNRS/ENSICAEN/UCBN, 6 boulevard du Maréchal Juin, 14050 Caen, France; E-Mails: bruma.alina@ensicaen.fr (A.B.); sylvie.malo@ensicaen.fr (S.M.)

* Author to whom correspondence should be addressed; E-Mail: Samuel.Bernard@univ-montp2.fr; Tel.: +33-467-149-159; Fax: +33-467-149-119.

Received: 30 April 2014; in revised form: 11 July 2014 / Accepted: 11 July 2014 / Published: 31 July 2014

Abstract: The spray-pyrolysis of borazine at 1400 °C under nitrogen generates boron nitride (BN) nanoparticles (NPs). The as-prepared samples form elementary blocks containing slightly agglomerated NPs with sizes ranging from 55 to 120 nm, a Brunauer-Emmett-Teller (BET)-specific surface area of 34.6 m^2 g^{-1} and a helium density of 1.95 g cm^{-3}. They are relatively stable in air below 850 °C in which only oxidation of the NP surface proceeds, whereas under nitrogen, their lower size affects their high temperature thermal behavior in the temperature range of 1450–2000 °C. Nitrogen heat-treated nanostructures have been carefully analyzed using X-ray diffraction, electron microscopy and energy-dispersive X-ray spectroscopy. The high temperature treatment (2000 °C) gives hollow-cored BN-NPs that are strongly facetted, and after ball-milling, hollow core-mesoporous shell NPs displaying a BET-specific surface area of 200.5 $m^2 \cdot g^{-1}$ and a total pore volume of 0.287 $cm^3 \cdot g^{-1}$ were produced. They have been used as host material to confine, then destabilize ammonia borane (AB), thus improving its dehydrogenation properties. The as-formed AB@BN nanocomposites liberated H_2 at 40 °C, and H_2 is pure in the temperature range 40–80 °C, leading to a safe and practical hydrogen storage composite material.

Keywords: borazine; BN; nanoparticles; ammonia borane; hydrogen storage

1. Introduction

Advanced nanostructured materials may be defined as materials having one dimension in the 1 to 100 nm range. The massive academic and industrial research efforts concerning these materials over the past decade arose from the remarkable variations in their physical and chemical properties when their dimension shrinks to the nanometric scale. In this category of materials, the interest for hexagonal-boron nitride (*h*-BN, but expressed here as BN) grew during the past few decades in relation to their unique combination of key properties.

BN is a synthetic chemical compound containing boron (B) and nitrogen (N) atoms in a one-to-one ratio. The in-plane atoms are linked through covalent bonds, while the out-of-plane layers are bonded by weak interactions (van der Waals forces) between B and N atoms, alternatively, providing anisotropic properties. BN displays a large band gap (~5.5 eV) and offers the lowest density (d = 2.26 g·cm^{-3}) among non-oxide ceramics. It proposes relatively good thermal stability in air and vacuum, high thermal conductivity, good thermal shock resistance, high electrical resistance, a low dielectric constant and loss tangent, microwave transparency, non-toxicity and easy machinability. Furthermore, it is non-abrasive, lubricating and non-reactive towards molten metals [1–6].

BN was obtained for the first time by Balmain [7] in 1842 through the reaction between boric oxide and potassium cyanide. It is nowadays produced by conventional powder technology, requiring nitridation or carbothermal reaction of boric acid/boric oxide with melamine or urea and the use of additives during the further sintering process [8]. It is used in various fields of chemistry, metallurgy, high temperature technology, electronics and in thermal management applications. However, beside the fact that the use of boric oxide inherently induces the presence of oxygen-containing phases, BN is only produced as powders with a plate-like morphology and workpieces. This inherently limits the development of BN.

Recently, interest at the academic level has arisen in both the synthesis of nanostructured BN and their applications for energy and the environment [9–13]. The important industrial challenges in line with nanostructured BN production requires the development of materials in which topologies, shapes and morphologies are tuned on demand. Inherent difficulties of traditional techniques to manufacture such materials can be addressed by the development of synthetic pathways where molecular/inorganic chemistry, processing and material chemistry/science are combined rationally to process BN with tailor-made properties [14]. The key step in nanostructured BN preparation is the selection of the BN precursors. Precursors with a good B:N ratio where/for which hydrogen (H) is the only element added to B and N are preferred. Borazine and derived polyborazylene are the most appropriate candidates [15,16]. Within this context, in this review article, we discuss the use of borazine (BZ) as a single-source molecular precursor used for the design of BN nanoparticles (NPs), hollow-cored BN-NPs that are strongly facetted and hollow core-mesoporous shell NPs. The latter have been used as host materials to encapsulate and store ammonia borane (AB).

2. Results and Discussion

2.1. Borazine-Derived BN Nanoparticles

Borazine (BZ) had been originally discovered by Alfred Stock in 1926 [17]. It displays a chemical formula $H_3B_3N_3H_3$. It is a preformed B-N-like ring structure and has the correct B-to-N ratio. Furthermore, it is economically competitive and attractive from a technical point of view, based on its reaction starting from cheap compounds, such as $(NH_4)_2SO_4$ and $(NaBH_4)$, reacting in tetraglyme at low temperature (120–140 °C) [18]. Borazine offers the advantage of being liquid with an adequate vapor pressure to be applied in gas phase pyrolysis processes to prepare nanostructured BN. As an illustration, we have demonstrated the interest of BZ to produce BN nanoparticles by spray-pyrolysis [19–22]. In our process, BZ is nebulized into an aerosol, and the stream consisting of tiny BZ droplets suspended in the carrier gas is transported by the carrier gas to be passed through the preheated tubular furnace at 1400 °C under nitrogen. In the hot-zone, the conversion of the nebulized precursor occurs through molecular condensation and ring-opening mechanisms involving the evolution of dihydrogen and producing vapors of BN ring-based species. The latter, reacting to form the consolidated boron nitride network, are swept by the nitrogen carrier-gas flow and, then, condensed into a white product getting collected into the cooling traps near the outlet of the furnace. The as-obtained product is stored inside an argon-filled glove-box. The scanning electron microscopy (SEM) images in Figure 1a show that the sample consists of particles with a relatively homogeneous size. This indicates that the most important operating factors, including the properties of the starting precursor, the pyrolysis temperature, the nitrogen flow rate, the residence time and heating rate of the droplet particles, are controlled during processing.

Figure 1. SEM (**a**), TEM (**b**) and HRTEM (**c**) images of samples obtained by spray-pyrolysis of borazine (BZ).

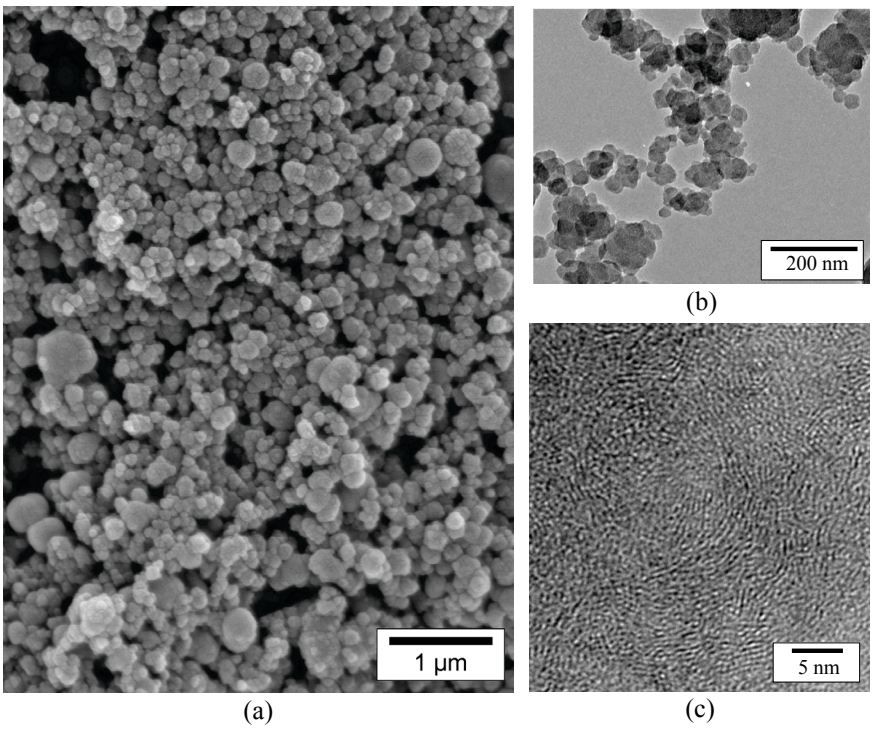

(a) (b) (c)

The low-magnification transmission electron microscope (TEM) bright field image of the sample (Figure 1b) show elementary blocks that are composed of slightly agglomerated nanoparticles (NPs). The particle size ranges from 55 to 120 nm. The high resolution TEM (HRTEM) image (Figure 1c) of the particle core demonstrates that the specimen consists of very fine BN crystallites in which sp^2 layers are significantly buckled in a disordered stacking sequence, exhibiting a size corresponding to less than six atomic basal planes, whereas their length does not exceed 50 Å. This points to the fact that BN is poorly crystallized similarly to a turbostratic structure. The TEM data are reinforced by the X-ray diffraction (XRD) experiments (Figure 2). The corresponding XRD patterns show very broad peaks at the *h*-BN (002), (100)/(101)/(004) and (110) positions. In particular, the (002) peak slightly shifts to lower angles in such samples, and the (100), (101) and (004) peaks merge into a single broad peak. Finally, the samples displayed a chemical formula of $B_{1.0}N_{0.9}$. Their specific surface area is 34.6 m^2 g^{-1}, and the helium density is 1.95 g cm^{-3}, as measured by Brunauer-Emmett-Teller (BET) and helium pycnometry, respectively.

Figure 2. XRD patterns of borazine-derived $B_{1.0}N_{0.9}$-NPs and annealed at a temperature ranging from 1450 to 2000 °C.

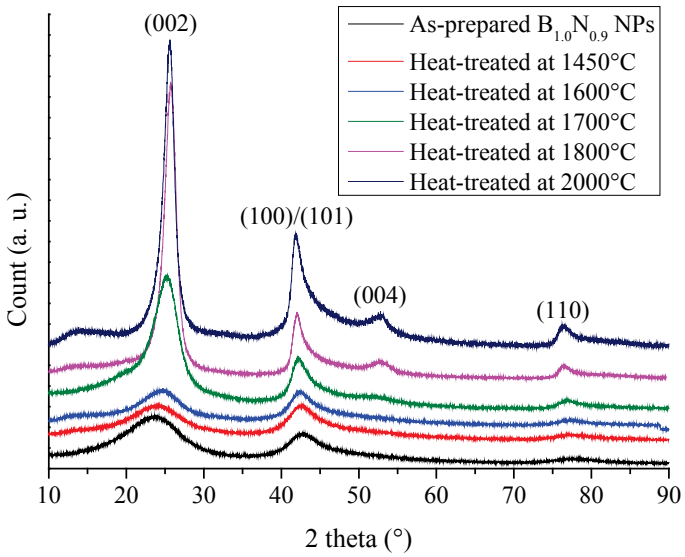

$B_{1.0}N_{0.9}$-NPs are stable in air below 850 °C in which only surface oxidation proceeds [21]. Here, we report the evolution of the nanostructural organization of $B_{1.0}N_{0.9}$-NPs in the temperature range of 1450–2000 °C under nitrogen. The XRD patterns in Figure 2 range from 10° to 90° for heat-treated $B_{1.0}N_{0.9}$-NPs.

The XRD patterns of samples heat-treated in the temperature range of 1450–1600 °C display features similar to the ones recorded for $B_{1.0}N_{0.9}$-NPs, indicating a turbostratic structure. For the sample annealed at 1700 °C, the (002) peak at 25.30° is sharpened, suggesting that the crystallite size became larger in the *c*-axis direction, although the shoulder-shaped broad feature remained on the low-angle side of the peak. This is also shown for the sharper (100)/(101)/(004) peak, which tends to be separated into the (004) peak and the (100)/(101) peak. The increase of the heat-treatment temperature to 1800 °C and 2000 °C resulted in an increased resolution of the XRD patterns. We can clearly distinguish the (002), (100)/(101), (004) and (110) peak positions. According to the sharpening

of the (002) and (100)/(101) peaks, we suggest that the crystallite size continuously increased in the *c*- and *a*-axes directions from 1400 °C to 2000 °C. However, no clear peaks corresponding to the (102) and (112) planes were observed. These findings tend to demonstrate that $B_{1.0}N_{0.9}$-NPs annealed at 2000 °C exhibit a turbostratic structure. The variation of the average crystallite size in the *c*-axis from the (002) peak ($\overline{L_c}$) and the interlayer d_{002} spacing of the samples during heat-treatment is shown in Figure 3. The dimension d_{002} is calculated from Bragg's law using the diffraction angle of the (002) peak. $\overline{L_c}$ represents the average number of stacked layers in the crystallites. The average stack height $\overline{L_c}$ is calculated from the Scherrer relation ($\overline{L_c} = 0.9\lambda(B^2 - B'^2)^{1/2}\cos\theta$, where λ is the $CuK_{\alpha 1}$ wavelength (λ = 0.1540 nm), θ the Bragg angle of the (002) diffraction peak, B the full width at half maximum intensity (FWHM) of the peak and B' the instrumental contribution).

Figure 3. Evolution of $\overline{L_{c(002)}}$ and d_{002} *vs.* annealing temperature.

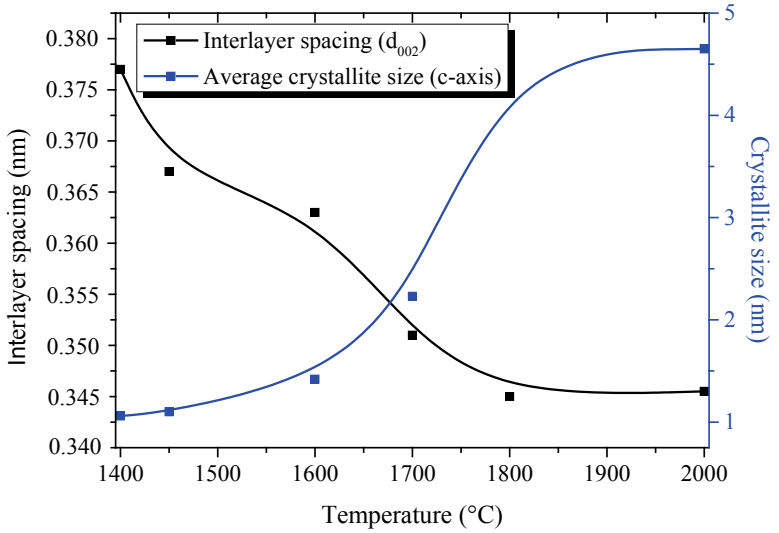

In the range of 1450 °C ($\overline{L_c}$ = 1.10 nm; d_{002} = 0.367 nm)–1600 °C ($\overline{L_c}$ = 1.42 nm; d_{002} = 0.363 nm), there is no major modification in both the apparent average grain size ($\overline{L_{c(002)}}$) and the value of the interlayer d-spacing d_{002}. Values are close to those calculated for as-prepared $B_{1.0}N_{0.9}$-NPs ($\overline{L_c}$ = 1.06 nm; d_{002} = 0.376 nm). This indicates a relatively high amount of disorder in the structure of the corresponding samples. At 1700 °C, the apparent average grain size increases slightly ($\overline{L_c}$ = 2.23 nm). Although the crystallization state in NPs heat-treated at 1700 °C is slightly improved, the BN phase remains poorly ordered as confirmed by the value of d_{002} (d_{002} = 0.351 nm), higher than that in a *h*-BN crystal (0.3327 nm). At 1800 °C, $\overline{L_c}$ increases to 4.63 nm and the interlayer d_{002} spacing is found to be 0.345 nm, which are values characteristic of a turbostratic phase. The minor changes in the XRD patterns of samples heat-treated at 2000 °C is reflected in the values of $\overline{L_c}$ (4.65 nm) and d_{002} (0.346 nm). In addition to XRD studies, we investigated TEM (Figure 4) and HRTEM (Figure 5) experiments to follow the evolution of the nanostructural organization in the temperature range of 1450–2000 °C.

Figure 4. TEM images of the samples annealed at (**a**) 1450 °C; (**b**) 1600 °C; (**c**) 1700 °C; (**d**) 1800 °C and (**e**) 2000 °C.

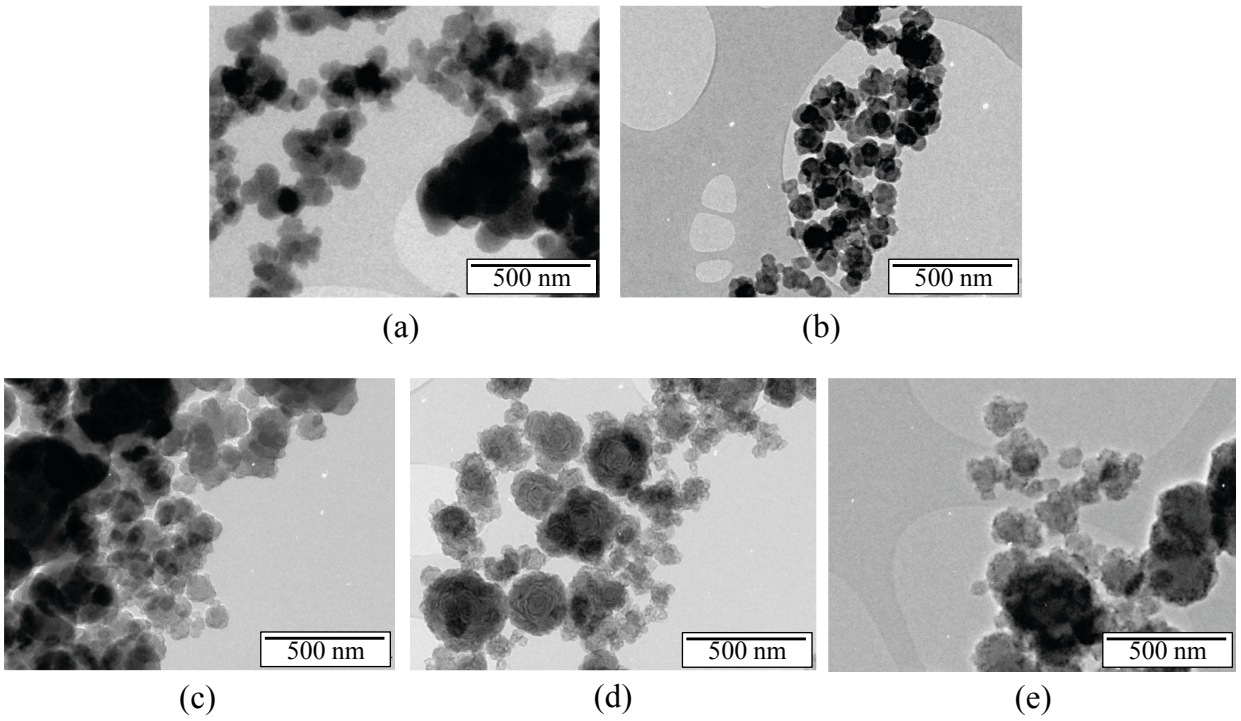

Figure 5. HRTEM images of the samples annealed at (**a**) 1450 °C; (**b**) 1600 °C; (**c**) 1700 °C; (**d**) 1800 °C; (**e**) 2000 °C; (**f**) evidence of a core-shell structure generated at 2000 °C.

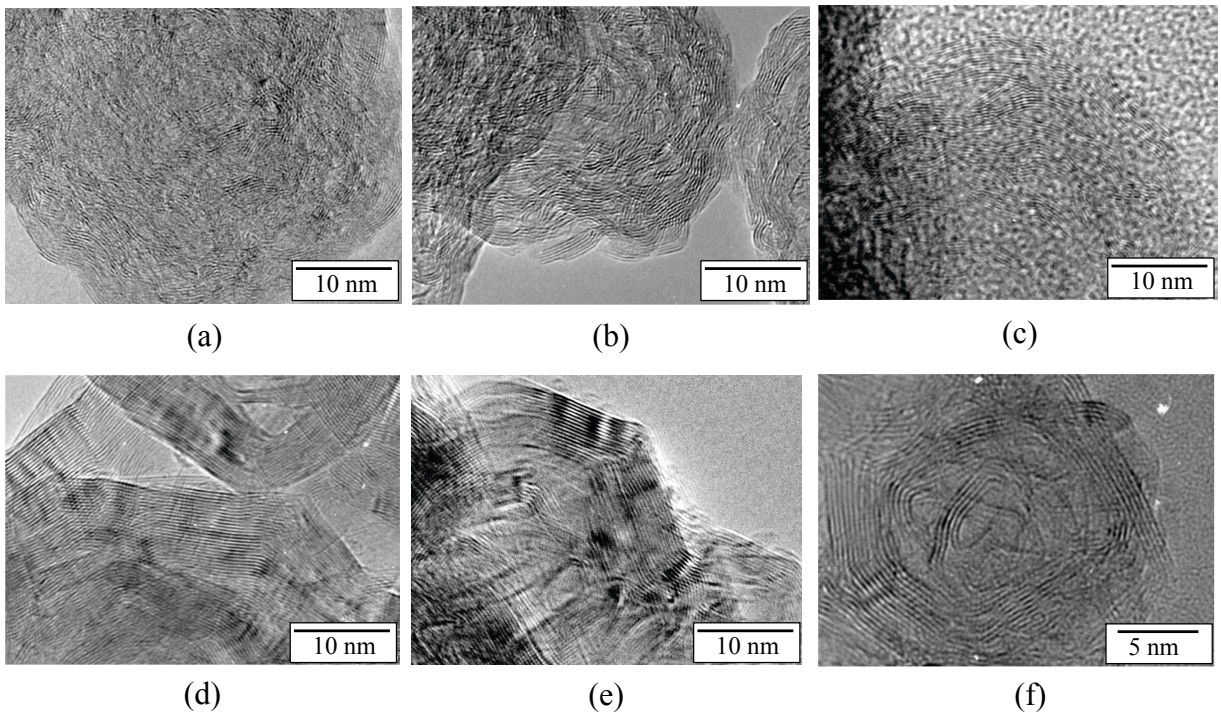

The annealed samples form elementary blocks composed of nanosized particles that are round in shape and slightly agglomerated. Both the average size of annealed particles and the agglomeration

seem to increase with the temperature of the annealing, which is in good agreement. This is clear for the samples annealed at 1800 °C (Figure 4d) and 2000 °C (Figure 4e), respectively. We therefore extended our analysis, by performing high resolution TEM (HRTEM), in order to refine/emphasize the structural information.

Figure 5 reports HRTEM images of the same samples.

Clear differences appear between the samples annealed in the range of 1450–2000 °C. After heat-treatment to 1450 °C (Figure 5a), the sample displays a turbostratic BN structure with more distinct (002) layers in comparison to the nanostructure observed in pristine $B_{1.0}N_{0.9}$-NPs (Figure 1c). In the sample annealed at 1600 °C (Figure 5b) and 1700 °C (Figure 5c), we can also observe the formation of nanodomains made of BN layers surrounding voids. The HRTEM image reveals the formation of concentric shelled nanodomains. The lattices of these BN nanostructures have a local interlayer spacing of 3.51 Å. Annealing at a temperature of 1800 °C (Figure 5d) and 2000 °C (Figure 5e,f) leads to hollow-cored BN-NPs that are strongly facetted, forming polygonal particles with an interlayer spacing of 3.34 Å. We investigated the potential of samples heat-treated at 2000 °C to confine H_2 storage materials.

2.2. Hydrogen Storage Applications

Ammonia borane (AB) is a white crystalline solid that was first prepared by Shore and Parry in 1955 [23]. Over the past decade, this compound has attracted considerable attention as portable hydrogen storage materials, according to its high gravimetric hydrogen contents (*ca.* 20% by weight) [24–29]. A very pertinent review dedicated to this compound and related derivatives as dihydrogen sources was proposed by Staubitz *et al.* in 2010 [29].

In the pristine state, AB is almost stable under inert conditions up to about 100 °C and decomposes within the range 100–200 °C through a two-step exothermic process where two equivalent H_2, as well as undesired by-products, such as borazine $B_3N_3H_6$ and NH_3, are evolved [24,25]. This decomposition suffers from three important problems: (1) the process is exothermic, which means that the storage reversibility is thermodynamically impossible in acceptable operating conditions; (2) the dehydrogenation temperature is too high for the portable/mobile application prospects; (3) the emission of undesired by-products is detrimental, as they are incompatible with the use of proton exchange membrane fuel cell (PEMFC) [27].

A promising solution seems to be the decrease of the particle size at the nanoscale (<10 nm) via confinement of the borane in a porous compound (*i.e.*, scaffold) [30]. As an illustration, Gutowska *et al*. showed that AB confined in the mesoporosity of silica SBA (Santa Barbara Amorphous)-15 has improved dehydrogenation behavior in comparison to the pristine hydride, with an onset at 70 °C and the liberation of borazine-free H_2 [31]. The destabilization of AB is generally explained by two phenomena. The first one is the nanosizing of the hydride particle. At the nanoscale, both kinetics and thermodynamics might be altered by both size and interface effects. In fact, the surface energy value could be different as a result of the interactions between the active confined material and the scaffold. The second phenomenon is associated with $H^{\delta+}\cdots H^{\delta-}$ surface interactions, with $H^{\delta-}$ of the BH_3 moiety of AB and $H^{\delta+}$ belonging to surface/terminal hydroxyl groups (–O–H) generally found on

carbonaceous or oxide nano-scaffolds. Such acid-base interactions enhance H_2 release, but usually lead to an unstable material at room conditions [25].

An improved strategy we recently demonstrated is to use nano-scaffolds free of reactive surface groups [22]. For that purpose, we used the $B_{1.0}N_{0.9}$-NPs annealed at 2000 °C, which we labeled $B_{1.0}N_{0.9}$-NP2000. As measured by energy dispersive X-ray spectrometry (EDX), boron, nitrogen and oxygen contents are 43.55, 55.7 and 0.75 wt%, respectively. Unfortunately, they exhibit a Brunauer-Emmett-Teller (BET)-specific surface area of 21.8 $m^2 \cdot g^{-1}$, which is low to achieve the nanoconfinement of AB. Therefore, we applied a ball-milling process of this sample to tentatively increase the specific surface area, leading to the sample labeled $B_{1.0}N_{0.9}$-NP2000BM. In comparison to $B_{1.0}N_{0.9}$-NP2000, the sample $B_{1.0}N_{0.9}$-NP2000BM shows a considerably increased BET-specific surface area with 200.5 $m^2 \cdot g^{-1}$ and a total pore volume of 0.424 $cm^3 \cdot g^{-1}$ as measured by the Barrett-Joyner-Halenda (BJH) analysis. As a result of the ball-milling, the HRTEM images (Figure 6a,b) of the sample showed that cleavage of the walls occurred through the basal planes. In addition, Figure 6c show that the stacking sequence can in some cases be disordered similarly to those of *t*-BN after ball-milling.

As a result of the BET and TEM investigations, we successfully demonstrated that the walls of the hollow-cored BN-NPs could be opened to provide porosity after ball-milling.

Figure 6. HRTEM images of the sample $B_{1.0}N_{0.9}$-NP2000BM evidencing in (**a**) and (**b**), a cleavage of the walls in the area delimited by the white arrows, and in (**c**), a disordering of the stacking sequence.

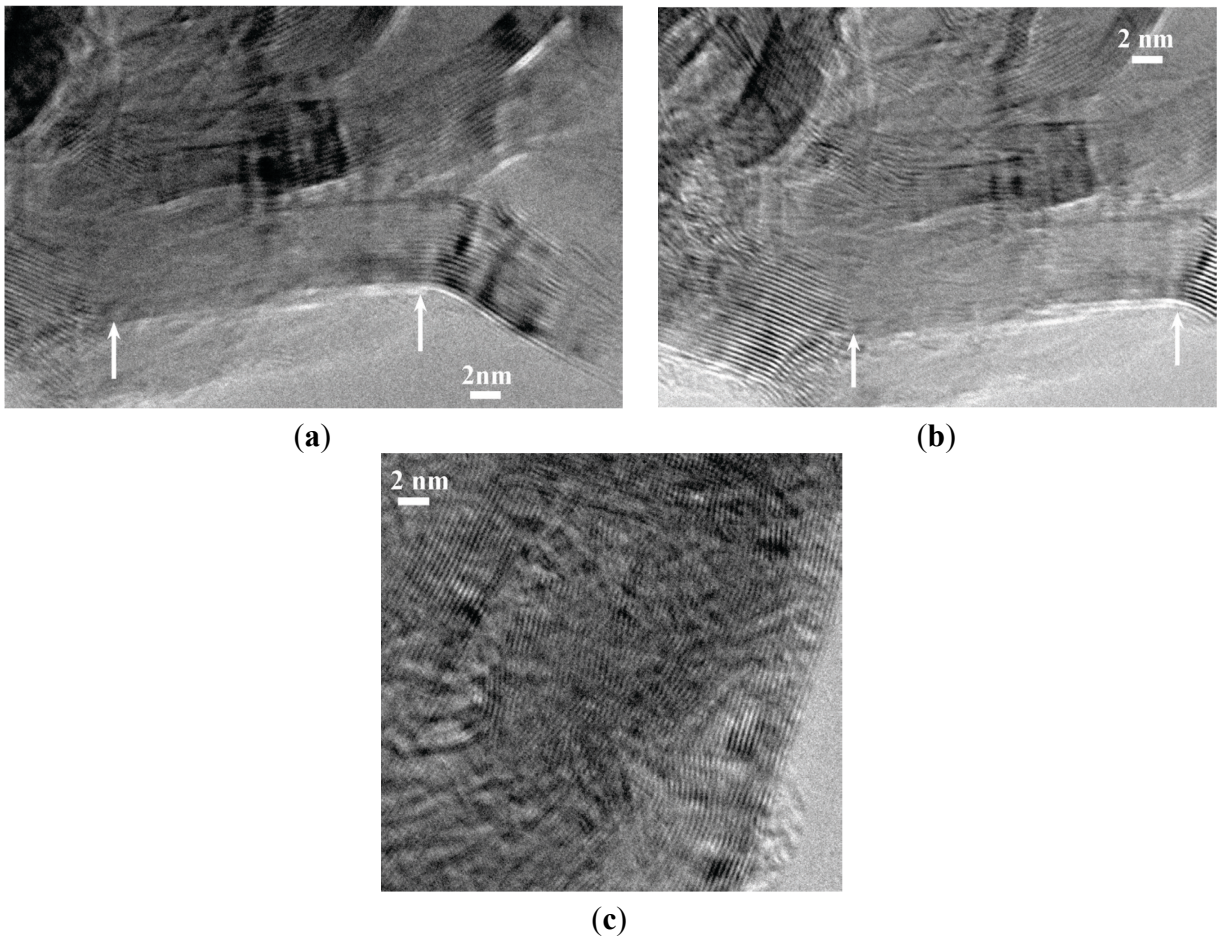

(**a**) (**b**)

(**c**)

Hydrogen storage materials can be confined within porous scaffolds by melt infiltration (if the active hydrogen storage material melts and do not decompose) or solution infiltration. In our procedure, a solution of AB in tetrahydrofuran (THF) was infiltrated into the framework of the sample $B_{1.0}N_{0.9}$-NP2000BM according to an optimized procedure described elsewhere [25]. A nanocomposite labeled AB@$B_{1.0}N_{0.9}$-NP2000BM was formed. It was stored at 3–4 °C. The successful impregnation of AB in $B_{1.0}N_{0.9}$-NP2000BM was followed by N_2 adsorption/desorption analysis of the nanocomposite. A BET-specific surface area of 6.7 $m^2 \cdot g^{-1}$ and a total pore volume of 0.023 $cm^3 \cdot g^{-1}$ are measured, which demonstrates that AB was inserted into the hollow core and blocked the pores of the nano-scaffolds. More interesting is that the decomposition of AB is down to 81 °C (compared to 110 °C for the pristine AB in our conditions) and that a major evolution of H_2 is identified by MS. In our experimental conditions, the only by-product was identified to be NH_3 above 80 °C. At 80 °C, a weight loss of 1.7 wt% was measured, which means an effective gravimetric hydrogen storage capacity of 3.4 wt% by considering a weight ratio equal to 1:1 in AB@$B_{1.0}N_{0.9}$-NP2000BM.

Our results confirmed the remarkable benefit of hollow-cored BN-NPs on the dehydrogenation behavior of AB. The performance is comparable to the dehydrogenation results of AB confined into a magnesium metal organic framework (MOF) [32,33] or nickel MOF [34], whereas only nanoconfinement is considered here. Most interesting, the MS results suggest that there is no detectable trace of borazine as a gaseous by-product. Another important observation standing from the thermogravimetric analysis coupled mass spectrometry (TGA-MS) result is that AB@$B_{1.0}N_{0.9}$-NP2000BM is stable at room conditions. Accordingly, the stability of AB@$B_{1.0}N_{0.9}$-NP2000BM at <40 °C is clearly attributed to the absence of surface $H^{\delta+}$, and the improvement of the dehydrogenation properties of AB in AB@$B_{1.0}N_{0.9}$-NP2000BM can be exclusively ascribed to the effect of nanoconfinement.

3. Experimental Section

The synthesis of borazine was carried out in an argon atmosphere, using argon/vacuum lines and Schlenk-type flasks. Argon (>99.995%) was purified by passing through successive columns of phosphorus pentoxide (Sigma-Aldrich, Saint Quentin, France), sicapent™ (Millipore S.A.S, Molsheim, France) and copper oxide-based catalysts (Sigma-Aldrich, Saint Quentin, France). The Schlenk flasks were dried at 120 °C overnight before pumping under vacuum and before filling with argon for the synthesis. Sodium borohydride ($NaBH_4$, ≥98.5%, powder from Sigma-Aldrich, Saint Quentin, France), ammonium sulfate ($(NH_4)_2SO_4$, ≥99.0% from Sigma-Aldrich (Saint Quentin, France) and tetraethylene glycol dimethyl ether($CH_3O(CH_2CH_2O)_4CH_3$, 99.0%, from Sigma-Aldrich (Saint Quentin, France) were used as-received. It should be mentioned that ammonium sulfate was dried at 120 °C inside an oven for three days, then put under vacuum during cooling for 1 h. Manipulation of the chemical products was made inside an argon-filled glove box (Jacomex BS521; Dagneux, France) dried with phosphorus pentoxide.

Borazine Synthesis: The operating procedure, adapted from the literature [18], was previously reported by our group [19]. FTIR (Caesium Iodide (CsI) windows/cm^{-1}): (N–H) = 3451 medium; (B–H) = 2509 medium; (B–N) = 1454 small; (B–N–B) = 897 medium. ^1H NMR

(300 MHz/$CDCl_3$/ppm): = 3.30–5.35 (quadruplet, 3H, B*H*), 5.35–6.05 (triplet, 3H, N*H*). ^{11}B NMR (96.29 MHz/C_6D_6/ppm): = 30.1 (br).

Nanoparticle Preparation: The experimental set-up is composed of a nebulized spray generator (RBI, Meylan, France), in which the spray is generated by a piezoelectric device (barium titanate). Frequency (800 kHz) and power (100 W) alimentations are adjusted to obtain the aerosol. The aerosol temperature is first held at 15 °C by a regulated water circulation to avoid borazine evaporation and/or condensation. The piezoelectric device generates an ultrasound beam, which is directed to the liquid-gas interface; a fountain formed at the surface followed by the generation of the spray, resulting from vibrations at the liquid surface and cavitations at the gas-liquid interface.

The borazine was directly introduced in the aerosol generating chamber under nitrogen, then aerosolized and carried to the pyrolysis furnace with a 0.5 $mL \cdot min^{-1}$ nitrogen flow rate. The thermal decomposition of borazine was performed in a hot alumina tube containing an isothermal zone of 0.1 m in length. The fast heating rate implies gaseous species generation leading to powder formation by a chemical vapor condensation route. The particles were finally trapped into two collectors placed before the vacuum pump and containing filter-barriers made of microporous alumina (pore size of 1 μm). Yield was estimated to be 0.22 $g \cdot min^{-1}$. After synthesis, the particles are stored inside an argon-filled glove-box. In a typical experiment, 27 mL (21.9 g) of borazine is used to produce 6.5 g of $B_{1.0}N_{0.9}$-NPs. However, the exact yield is difficult to estimate, because of the design of the spray-pyrolysis system. A non-negligible/considerable quantity of powders, deposited in the furnace tube, cannot be recovered. To study the evolution of their crystallization degree, 2 g of the $B_{1.0}N_{0.9}$-NPs are placed into boron nitride boats and then introduced in a graphite furnace (Gero 5 Model HTK 8). The furnace chamber is subsequently suctioned with a pump charged with nitrogen before heating. A cycle of ramping at 10 $°C.min^{-1}$ is used to heat the sample to the desired temperature (in the range 1400–2000 °C) with a holding time of 1 h, before cooling down to RT at 10 $°C \cdot min^{-1}$. Chemical analysis found (wt%): B, 50.0; N, 49.4; O, 0.6. The milling process of $B_{1.0}N_{0.9}$-NP2000 is performed under inert condition (argon) with a planetary ball-miller (Retsch PM100; Haan, Germany). The described process has been optimized (in terms of mass, ratio balls/BN, time, rotation) to our conditions. Typically, degassed $B_{1.0}N_{0.9}$-NP2000 (at 150 °C under dynamic vacuum for 24 h) is introduced into a stainless steel reactor (25 mL). Balls in stainless steel are added (weight ratio balls: $B_{1.0}N_{0.9}$-NP2000 of 20). The milling process is performed at 600 rpm for 1 h. The as-obtained $B_{1.0}N_{0.9}$-NP2000BM is finally sieved.

The infiltration of ammonia borane is performed as follows: the host material $B_{1.0}N_{0.9}$-NP2000BM (100 mg) is degassed at 150 °C under dynamic vacuum for 24 h in a Schlenk tube and then cooled to 0 °C. In an argon-filled glove box, a concentrated solution of ammonia borane (100 mg, 97%; Sigma Aldrich, Saint Quentin, France) is prepared using 0.5 mL of anhydrous THF (Sigma Aldrich, Saint Quentin, France). The ammonia borane solution is injected into the Schlenk tube containing $B_{1.0}N_{0.9}$-NP2000BM kept under static vacuum and at 0 °C. By capillary action, the ammonia borane solution fills the channels of the host rapidly, which is evidenced by vigorous effervescence. When the effervescence stops, the sample is put under ultrasonic treatment for 20 min at 0 °C. Finally, the as-obtained sample AB@$B_{1.0}N_{0.9}$-NP2000BM (weight ratio $B_{1.0}N_{0.9}$-NP2000BM:AB of 1) is dried under dynamic vacuum for 48 h at 0 °C. The composite samples obtained are denoted AB@$B_{1.0}N_{0.9}$-NP2000BM. Samples are transferred in an argon-filled vial and then stored in a fridge at 3–4 °C.

Characterizations: The $B_{1.0}N_{0.9}$-NPs and annealed samples are first mounted on carbon film-covered stainless pads for scanning electron microscopy (SEM, Hitachi S4800, Tokyo, Japan) including Energy Dispersive X-ray Spectroscopy (EDX, EDAX/TSL Genesis 4000, Tokyo, Japan). Due to the insulating properties of BN, the samples are sputtered with 10 nm of a Pd/Au mixture to prevent charging during SEM observations. In parallel, the same samples are ultrasonicated in ethanol, and the resulting solution is afterwards deposited on a collection of hollow carbon-film-covered copper grids for transmission electron microscopy (TEM, TOPCON 002B working at 200 kV, Tokyo, Japan) observation. Samples were characterized using a Philips PW 3040/60 X'Pert PRO X-ray diffraction system (Eindhoven, The Netherland). Powder samples are prepared by placing ~100 mg on the XRD sample holder (PVC), and the sintered pieces were put down on the XRD sample holder for data collection. Cu Kα (λ = 1.54 Å) radiation with a Ni filter was used with a working voltage and a current of 40 kV and 30 mA, respectively. Scans were continuous from 2θ = 10°–90° with a time per step of 0.85 s in increments of 0.017°. Peak positions and relative intensities were characterized by comparison with JCPDS (Joint Committee on Powder Diffraction Standards) files of the standard material (JCPDS card No 34-0421). Debye-Scherrer line broadening was used to calculate the average crystallite sizes from each XRD pattern. The transmission electron microscopy (TEM) studies of $B_{1.0}N_{0.9}$-NP2000BM samples were carried out with a JEOL (Tokyo, Japan) GmbH 2010F transmission electron microscope (Cs = 1 mm) operating at 200 kV. The characterization of the samples was performed by N_2 adsorption/desorption (Sorptomatic 1990 Series, Thermo Fisher Scientific Inc, Waltham, MA, USA). Thermogravimetric analysis (TGA) measurements (repeated at least three times to ensure the reproducibility of the results) were performed with a Mettler Toledo TGA/SDTA 851e (Schwerzenbach, Switzerland) under the following conditions: sample mass 9–10 mg, aluminum crucible of 100 µL with a pinhole, heating rate of 5 °C·min^{-1}, temperature range 25–200 °C and atmosphere of N_2 (60 mL·min^{-1}). The purity of H_2 was analyzed by mass spectrometry (Canon Anelva Corporation MQA200TS, Tokyo, Japan) coupled to the TGA apparatus.

4. Conclusions

This article reviews our recent advancements in the synthesis and energy application of nanostructured boron nitride. Such materials exhibit chemical and physical properties that are significantly different from those of bulk and microsized materials. In our approach, we discussed our recent strategy based on borazine, which has been used as a vapor phase pyrolysis precursor for the synthesis and fabrication of BN nanoparticles. In particular, we demonstrated the possibility of tailoring the nanostructure of these nanoparticles by a further annealing process at high temperature (2000 °C), leading to hollow-cored BN-NPs that are strongly facetted, forming polygonal particles with an interlayer spacing of 3.34 Å. The ball-milling of these nanostructures allowed developing the specific surface area of the material while hollow-cored BN-NPs porous shell structures were obtained. They show a BET-specific surface area of 200.5 $m^2 \cdot g^{-1}$, a total pore volume of 0.287 $cm^3 \cdot g^{-1}$ and a narrow pore size distribution centered at 3.5 nm. They were used as nano-scaffolds of ammonia borane in order to improve its dehydrogenation properties to form a nanocomposite able to liberate pure H_2 in the temperature range 40–80 °C in our conditions. The only trace of by-product being detected at >80 °C is ammonia. Considering the regenerability of ammonia borane [35], our results suggest that

our composite material is a safe and practical hydrogen storage material. This improvement is exclusively ascribed to the nanoconfinement effect.

Acknowledgments

The authors acknowledge Vincent Salles for spray-pyrolysis and Arnaud Brioude for the TEM observation of nanoparticles and samples annealed in the temperature range of 1450–2000 °C before ball-milling.

Author Contributions

The findings in this manuscript are part of Georges Moussa thesis work. Chrystelle Salameh performed borazine synthesis. Philippe Miele, Umit B. Demirci and Samuel Bernard advised the thesis and directed the research. Alina Bruma and Sylvie Malo guided the TEM experiments of the sample $B_{1.0}N_{0.9}$-NP2000BM. The manuscript was written through contributions of all authors. All authors have given approval to the final version of the manuscript.

Conflicts of Interest

The authors declare no conflict of interest.

References

1. Paine, R.T.; Narula, C.K. Synthetic route to boron nitride. *Chem. Rev.* **1990**, *90*, 73–91.
2. Wu, J.; Han, W.-Q.; Walukiewicz, W.; Ager, J.W., III; Shan, W.; Haller, E.E.; Zettl, A. Raman spectroscopy and time-resolved photoluminescence of BN and $B_xC_yN_z$ nanotubes. *Nano Lett.* **2004**, *4*, 647–650.
3. Watanabe, K.; Tanigushi, T.; Kanda, H. Direct-bandgap properties and evidence for ultraviolet lasing of hexagonal boron nitride single crystal. *Nat. Mater.* **2004**, *3*, 404–409.
4. Kubota, Y.; Watanabe, K.; Tsuda, O.; Tanigushi, T. Deep ultraviolet light-emitting hexagonal boron nitride synthesized at atmospheric pressure. *Science* **2007**, *317*, 932–934.
5. Macnaughton, J.B.; Moewes, A.; Wilks, R.G.; Zhou, X.T.; Sham, T.K.; Tanigushi, T.; Watanabe, K.; Chan, C.Y.; Zhang, W.J.; Bello, I.; *et al.* Electronic structure of boron nitride single crystals and films. *Phys. Rev. B* **2005**, *72*, 195113:1–195113:8.
6. Zhong, W.; Wang, S.; Li, J.; Bechelany, M.C.; Ghisleni, R.; Rossignol, F.; Balan, C.; Chartier, T.; Bernard, S.; Miele, P.; *et al.* Design of carbon fibre reinforced boron nitride matrix composites by vacuum-assisted polyborazylene transfer moulding and pyrolysis. *J. Eur. Ceram. Soc.* **2013**, *33*, 2979–2992.
7. Balmain, W.H. Bemerkungen über die Bildung von Verbindungen des Bors und Siliciums mit Stickstoff und gewissen Metallen. *J. Prakt. Chem*. **1842**, *27*, 422–430 (In German).
8. Lipp, A.; Schwetz, K.A.; Hunold, K. Hexagonal boron nitride: Fabrication, properties and applications. *J. Eur. Ceram. Soc.* **1989**, *5*, 3–9.
9. Lei, W.; Portehault, D.; Liu, D.; Qin, S.; Chen, Y. Porous boron nitride nanosheets for effective water cleaning. *Nat. Commun.* **2013**, *4*, 1777–1783.

10. Rousseas, M.; Goldstein, A.P.; Mickelson, W.; Worsley, M.A.; Woo, L.; Zettl, A. Synthesis of highly crystalline sp2-bonded boron nitride aerogels. *ACS Nano* **2013**, *7*, 8540–8546.
11. Li, J.; Xiao, X.; Xu, X.; Lin, J.; Huang, Y.; Xue, Y.; Jin, P.; Zou, J.; Tang, C. Activated boron nitride as an effective adsorbent for metal ions and organic polluants. *Nature* **2013**, *3*, 3208–3214.
12. Weng, Q.; Wang, X.; Zhi, C.; Bando, Y.; Golberg, D. Boron nitride porous microbelts for hydrogen storage. *ACS Nano* **2013**, *7*, 1558–1565.
13. Siria, A.; Poncharal, P.; Biance, A.-L.; Fulcrand, R.; Blasé, X.; Purcell, S.T.; Bocquet, L. Giant osmotic energy conversion measured in a single transmembrane boron nitride nanotube. *Nature* **2013**, *494*, 455–458.
14. Bernard, S. *Design, Processing and Properties of Ceramic Materials from Preceramic Precursors in Materials Science and Technologies*; Nova Publishers: New York, NY, USA, 2012.
15. Alauzun, J.G.; Ungureanu, S.; Brun, N.; Bernard, S.; Miele, P.; Backov, R.; Sanchez, C. Novel Monolith-type Boron Nitride Hierarchical Foams Obtained through Integrative Chemistry. *J. Mater. Chem.* **2011**, *21*, 14025–14030.
16. Termoss, H.; Toury, B.; Payan, S.; Brioude, A.; Bernard, S.; Cornu, D.; Vallette, S.; Benayoun, S.; Miele, P. Preparation of boron nitride-based coatings on metallic substrates via infrared irradiation of dip-coated polyborazylene. *J. Mater. Chem.* **2009**, *19*, 2671–2674.
17. Stock, A.; Pohland, E. Borwasserstoffe, IX.: $B_3N_3H_6$. *Ber. Dtsch. Chem. Ges.* **1926**, *59(B)*, 2215–2223 (In German).
18. Wideman, T.; Sneddon, L.G. Convenient procedures for the laboratory preparation of borazine. *Inorg. Chem.* **1995**, *34*, 1002–1003.
19. Salles, V.; Bernard, S.; Li, J.; Brioude, A.; Chehaidi, S.; Foucaud, S.; Miele, P. Design of Highly Dense Boron Nitride by the Combination of Spray-Pyrolysis of Borazine and Additive-free Sintering of Derived Ultrafine Powders. *Chem. Mater.* **2009**, *21*, 2920–2929.
20. Bernard, S.; Salles, V.; Li, J.; Brioude, A.; Bechelany, M.; Demirci, U.B.; Miele, P. High-Yield Synthesis of Hollow Boron Nitride Nano-Polyhedrons. *J. Mater. Chem.* **2011**, *21*, 8694–8699.
21. Salles, V.; Bernard, S.; Chiriac, R.; Miele, P. Structural and Thermal Properties of Boron Nitride Nanoparticles. *J. Eur. Ceram. Soc.* **2012**, *32*, 1867–1871.
22. Moussa, G.; Demirci, U.B.; Malo, S.; Bernard, S.; Miele, P. Boron Nitride Nanopolyhedrons with hollow core@Mesoporous Shell structure: From Design to solid-state hydrogen storage application. *J. Mater. Chem. A* **2014**, *2*, 7717–7722.
23. Shore, S.G.; Parry, R.W. The crystalline compound ammonia boraone H_3NBH_3. *J. Am. Chem. Soc.* **1955**, *77*, 6084–6085.
24. Demirci, U.B.; Bernard, S.; Chiriac, R.; Toche, F.; Miele, P. Hydrogen release by thermolysis of ammonia borane NH_3BH_3 and then hydrolysis of its by-product [BNH_x]. *J. Power Sources* **2011**, *196*, 279–286.
25. Moussa, G.; Bernard, S.; Demirci, U.B.; Chiriac, R.; Miele, P. Room-temperature hydrogen release from activated carbon-confined ammonia borane. *Int. J. Hydr. Energy* **2012**, *37*, 13437–13445.
26. Stephens, F.H.; Pons, V.; Baket, R.T. Ammonia-Borane: The Hydrogen Source par excellence. *Dalton Trans.* **2007**, 2613–2626.
27. Hamilton, C.W.; Baker, R.T.; Staubitz, A.; Manners, I. B–N compounds for chemical hydrogen storage. *Chem. Soc. Rev.* **2009**, *38*, 279–293.

28. Sanyal, U.; Demirci, U.B.; Jagirdar, B.R.; Miele, P. Hydrolysis of ammonia borane as hydrogen source: Fundamental issues and potential solutions towards implementation. *ChemSusChem.* **2011**, *4*, 1731–1739.
29. Staubitz, A.; Robertson, A.P.M.; Manners, I. Ammonia-borane and related compounds as dihydrogen sources. *Chem. Rev.* **2010**, *110*, 1079–1124.
30. De Jong, P.E.; Adelhelm, P. Nanosizing and nanoconfinement: New strategies towards meeting hydrogen storage goals. *ChemSusChem.* **2010**, *3*, 1332–1348.
31. Gutowska, A.; Li, L.; Shin, Y.; Wang, C.M.; Li, X.S.; Linehan, J.C.; Smith, R.S.; Kay, B.D.; Schmid, B.; Shaw, W.; *et al.* Nanoscaffold Mediates Hydrogen Release and the Reactivity of Ammonia Borane. *Angew. Chem. Int. Ed*. **2005**, *44*, 3578–3582.
32. Gadipelli, S.; Ford, J.; Zhou, W.; Wu, H.; Udovic, T.J.; Yildirim, T. Nanoconfinement and catalytic dehydrogenation of ammonia borane by magnesium-metal-organic-framework-74. *Chem. Eur. J.* **2011**, *17*, 6043–6047.
33. Srinivas, G.; Travis, W.; Ford, J.; Wu, H.; Guo, Z.-X.; Yildirim, T. Nanoconfined ammonia borane in a flexible metal–organic framework Fe–MIL-53: Clean hydrogen release with fast kinetics. *J. Mater. Chem. A* **2013**, *1*, 4167–4172.
34. Peng, Y.; Ben, T.; Jia, Y.; Yang, D.; Zhao, H.; Qiu, S.; Yao, X. Dehydrogenation of Ammonia Borane Confined by Low-Density Porous Aromatic Framework. *J. Phys. Chem. C* **2012**, *116*, 25694.
35. Sutton, A.D.; Burrell, A.K.; Dixon, D.A.; Garner, E.B., III; Gordon, J.C.; Nakagawa, T.; Ott, K.C.; Robinson, J.P.; Vasiliu, M. Regeneration of ammonia borane spent fuel by direct reaction with hydrazine and liquid ammonia. *Science* **2011**, *331*, 1426–1429.